Title

Bayesian parameter estimation for the inclusion of uncertainty in progressive damage simulation of composites.

Authors

Reiner, Johannes

Linden, Nathaniel

Vaziri, Reza

et al.

Publication Date

2023-10-01

DOI

10.1016/j.compstruct.2023.117257

Peer reviewed

HHS Public Access

Author manuscript

Compos Struct. Author manuscript; available in PMC 2024 October 01.

Published in final edited form as:

Compos Struct. 2023 October 01; 321: . doi:10.1016/j.compstruct.2023.117257.

Bayesian parameter estimation for the inclusion of uncertainty in progressive damage simulation of composites

Johannes Reiner[a,*], **Nathaniel Linden**[b], **Reza Vaziri**[c], **Navid Zobeiry**[d], **Boris Kramer**[b]

[a]School of Engineering, Faculty of Science Engineering and Built Environment, Deakin University, Geelong, Australia

[b]Department of Mechanical and Aerospace Engineering, University of California San Diego, La Jolla, CA, USA

[c]Composites Research Network, Departments of Civil Engineering and Materials Engineering, The University of British Columbia, Vancouver, Canada

[d]Materials Science & Engineering Department, University of Washington, Seattle, USA

Abstract

Despite gradual progress over the past decades, the simulation of progressive damage in composite laminates remains a challenging task, in part due to inherent uncertainties of material properties. This paper combines three computational methods — finite element analysis (FEA), machine learning and Markov Chain Monte Carlo — to estimate the probability density of FEA input parameters while accounting for the variation of mechanical properties. First, 15,000 FEA simulations of open-hole tension tests are carried out with randomly varying input parameters by applying continuum damage mechanics material models. This synthetically-generated data is then used to train and validate a neural network consisting of five hidden layers and 32 nodes per layer to develop a highly efficient surrogate model. With this surrogate model and the incorporation of statistical test data from experiments, the application of Markov Chain Monte Carlo algorithms enables Bayesian parameter estimation to learn the probability density of input parameters for the simulation of progressive damage evolution in fibre reinforced composites. This methodology is validated against various open-hole tension test geometries enabling the determination of virtual design allowables.

[*]Corresponding author. johannes.reiner@deakin.edu.au (J. Reiner).

CRediT authorship contribution statement

Johannes Reiner: Conceptualization, Methodology, Software, Formal analysis, Investigation, Data curation, Writing – original draft, Writing – review & editing. **Nathaniel Linden:** Methodology, Software, Formal analysis, Investigation, Writing – original draft, Writing – review & editing. **Reza Vaziri:** Conceptualization, Writing – original draft, Writing – review & editing. **Navid Zobeiry:** Conceptualization, Methodology, Software, Formal analysis, Investigation, Data curation, Writing – original draft, Writing – review & editing. **Boris Kramer:** Conceptualization, Methodology, Investigation, Data curation, Writing – original draft, Writing – review & editing.

Declaration of competing interest

The authors declare that they have no known competing financial interests or personal relationships that could have appeared to influence the work reported in this paper.

Keywords

Finite element analysis; Machine learning; Markov chain Monte Carlo; Open-hole tension

1. Introduction

Despite many superior properties of Fibre Reinforced Polymers (FRPs) such as high strength-to-weight ratio or damage resistance, these materials typically suffer from a wide range of variability in their mechanical properties. These variations mainly arise from manufacturing-induced defects and imperfections such as fibre misalignment, inhomogeneous fibre volume fraction and local wrinkling [1]. Even state-of-the-art automated manufacturing processes such as automated fibre placement or tape laying induce defects resulting in a wide range of mechanical properties in the final composite product [2,3].

It is important to acknowledge these variations in properties when designing FRP composites. Therefore, statistical material data is required beyond simple average values [4]. For the certification of FRP composites in structural aerospace applications, industry must rely on the building-block approach for which comprehensive and costly testing programs must be undertaken in order to guarantee safe and reliable use of FRP composite structures and to obtain statistically meaningful properties. Design allowables evaluate confidence intervals to account for uncertainties and to include safety factors [5]. Depending on the application, some structural design allowables require empirical determination at higher testing levels at the sub-component or component level of the building block as they may be dependent on design geometry and specific manufacturing processes [6].

Finite element (FE) simulations promise a significant reduction in cost and time to develop and deploy lightweight FRP materials by predicting their mechanical behaviour before manufacturing and physical testing. FE models enable the simulation of large-scale structures at higher levels of the building block. Progressive damage simulation of FRP composites by means of Finite Element Analysis (FEA) has matured over the past couple of decades [7]. Various damage modelling techniques are nowadays available as built-in tools in commercial FE software packages ranging from continuum damage mechanics-based material models [8–10] to discrete techniques such as the cohesive zone method [11,12] or X-FEM [13].

The particular focus of the current work is Continuum Damage Mechanics (CDM) which incorporates damage in a smeared manner through the progressive reduction of the local material stiffness while maintaining the continuity of the FE mesh. The first CDM-based simulations of FRP composites date back to early 1990’s [14,15]. Due to its ease of implementation and computational efficiency, CDM has become a popular framework for the prediction of damage progression. Examples of applications of CDM to FRPs are the simulation of axial crushing of braided tubes [16,17], the prediction of fibre-kinking [18] or the simulation of notched laminates under tension [19–21].

Irrespective of the preferred damage modelling technique, one key question is how to consider the inherent uncertainties and variabilities in mechanical properties of FRP composites [22]. One method to include uncertainty into FE modelling of FRP composites is to model the inputs as random variables with specific probability densities. As an example, normal or Weibull distributions are assumed for fibre diameters or strength values depending on the length scale of interest in [23–25]. Uncertainty can also be incorporated into FEA by considering spatial variability throughout the FE mesh [26]. For example, Bavel et al. [1] assume spatial distributions for fibre misalignment, fibre volume fraction and fibre strength to simulate FRP composites subjected to tensile loads. Although some of the chosen distributions can be well justified through experimental measurements and physical observation, most of the uncertainty models on FRP composites require a-priori knowledge of these distributions [27].

A more general approach to model uncertainty of the inputs is to take a Bayesian perspective, which considers parameters to be random variables without assigning a particular probability density to them. Bayesian parameter estimation aims to determine the unknown probability density function (pdf) for each input parameter, called the *posterior density*, henceforth called the *posterior*, based on the available statistical data (ideally from physical tests). The advantage of Bayesian approaches comes from their ability to characterise the entire posterior and, thus, to quantify the uncertainty in parameter estimates via credible intervals [28–30]. Markov Chain Monte Carlo (MCMC) is one of the most popular methods for Bayesian parameter estimation. In order to efficiently characterise posteriors, MCMC algorithms construct a Markov chain of parameter samples that will be distributed according to the posterior in the long-sample limit. A frequent bottleneck when using MCMC is the need for a large number of model evaluations. Thus, high-fidelity FEA models alone are not efficient enough to be used inside Bayesian methods when expecting a reasonable turnaround time or given a limited computational budget. Therefore, this paper develops FE-informed Machine Learning (ML) surrogate models for FRP composites on the basis of previous work by the authors [31–33]. These ML surrogates provide fast model evaluations, making it feasible to apply Bayesian parameter estimation for the simulation of progressive damage in FRP composites.

Many fields across computational science, engineering and statistics develop and apply Bayesian methods [28,29,34,35]; however, few works in materials science have applied Bayesian parameter estimation. For example, Adeli et al. [36] calibrated a visco-plastic damage model to simulate metallic structures. Similarly, Joshi et al. [37] investigated the Bayesian estimation of hyperelastic properties, while Wu et al. [38] identified input parameters for a phase field damage model to simulate cement mortar materials.

This paper combines three computational methods — FEA, ML, and MCMC — to find the probability density of each FE input parameter to simulate the statistical response of FRP composites subjected to open-hole tensile tests. Easy-to-use and built-in features in commercial and open-source software are used in each computational method. The novelty and impact of the work lies in the unique combination of the three methods applied to FRP composites. Fig. 1 provides a graphical overview describing the interplay between the different methods. Section 2 outlines Bayesian parameter estimation and describes each

computational method. The results of the Bayesian estimation of input parameters are shown in Section 3 and are validated in Section 4. The discussion in Section 5 focuses on benefits and limitations of this study, and future work is concluded in Section 6.

2. Methodology

This section describes the underlying theories and computational methods to enable Bayesian parameter estimation for the simulation of progressive damage in FRP composites. In Section 2.1, we discuss Bayes' rule that is at the core of learning the posterior of the parameters. Section 2.2 describes the statistical test data obtained from open-hole tensile tests of FRP composites. The three computational methods — FEA, ML, and MCMC — are presented in Sections 2.3–2.5, respectively.

2.1. Bayes' rule

Given random input parameters $\boldsymbol{\theta} = (\theta_1, \theta_2, \ldots)^T$ of a CDM-based FE model, Bayesian parameter estimation determines the posterior pdf $p(\boldsymbol{\theta}|\boldsymbol{y})$ of the inputs conditioned on the data. In this work, the test data $\boldsymbol{y}$ is given by statistical results obtained from experimental open-hole tension tests on FRP composites. The posterior density can be calculated by Bayes' rule [29,39] as

$$p(\boldsymbol{\theta} \mid \boldsymbol{y}) = \frac{p(\boldsymbol{\theta})p(\boldsymbol{y} \mid \boldsymbol{\theta})}{p(\boldsymbol{y})} \tag{1}$$

where $p(\boldsymbol{\theta})$ is the prior density, henceforth called the prior, and $p(\boldsymbol{y}|\boldsymbol{\theta})$ the likelihood function. Under the assumption that the data follow a normal distribution $\boldsymbol{y} \sim \mathcal{N}(\boldsymbol{\mu}, \boldsymbol{\Sigma})$, with mean $\boldsymbol{\mu}$ and covariance $\boldsymbol{\Sigma}$, the likelihood function becomes

$$p(\boldsymbol{y} \mid \boldsymbol{\theta}) = \mathcal{N}((\boldsymbol{y} - \mathcal{M}(\boldsymbol{\theta})), \boldsymbol{\Sigma}), \tag{2}$$

where $\mathcal{M}(\boldsymbol{\theta})$ is the model evaluation (and later we will use $\mathcal{M}_{\mathrm{FEA}}(\boldsymbol{\theta})$ and $\mathcal{M}_{\mathrm{ML}}(\boldsymbol{\theta})$ to distinguish between FEM and ML models). The probability of the test data $p(\boldsymbol{y})$ can be treated as a normalising factor because it does not depend on $\boldsymbol{\theta}$.

2.2. Test data

The test data $\boldsymbol{y}$ is retrieved from the statistical test program on Open-Hole Tension (OHT) tests on IM7/8552 Carbon Fibre Reinforced Polymers (CFRPs) as part of the Composites Material Handbook CMH-17, see [6]. A standard OHT sample after testing is shown in Fig. 2(a) alongside the corresponding stress–strain curve in Fig. 2(b). Typically, CFRPs show brittle failure with a linear elastic increase in stress before failing abruptly. Due to such brittle behaviour, only strength data S_{OHT} is recorded.

As part of the comprehensive CMH-17 test program in [6], 30 samples of quasi-isotropic $[45/0/-45/90]_{2s}$ IM7/8552 laminates from seven batches were subjected to OHT tests at room temperature. Fig. 3 shows the spread of OHT strength values obtained from these 30 tests. A normal distribution $\boldsymbol{y} \sim \mathcal{N}(417, 14.7)$ is fitted to this data with a mean of 417 MPa and a standard deviation of 14.7 MPa (3.54% CoV). This data provides the statistical experimental results to evaluate Eq. (1).

2.3. Finite element analysis

The quasi-isotropic $[45/0/-45/90]_{2s}$ CFRP laminate is modelled using the isotropic coupled damage-plasticity material model MAT81 in the commercial FE software LS-DYNA. As inputs, the model requires elastic laminate properties such as Young's modulus E and Poisson's ratio ν as well as damage properties such as yield stress σ_{peak} and damage evolution parameters as a function of the effective plastic strain. Here, we consider linear softening where the post-peak response is characterised by the fracture energy G_f. This results in a representative stress–strain relation shown in Fig. 4. It is assumed that damage initiation at the damage initiation strain ε^i coincides with the onset of yielding in order to replicate brittle damage without the presence of plasticity. This assumption is motivated by the inherently brittle failure behaviour of FRPs. Therefore the four input parameters E, ν, ε^i and G_f are sufficient to define this laminate-based progressive damage model. This is similar to the manner in which the MAT81 material model in LS-DYNA was used in previous studies involving progressive damage simulation of quasi-isotropic composite laminates [10,31,32,41–44].

Fig. 5 shows the geometry and mesh of the FE model with the prescribed boundary conditions to simulate OHT tests of the quasi-isotropic $[45/0/-45/90]_{2s}$ IM7/8552 laminates. The size of the FE mesh as shown in Fig. 5 is 1 mm × 1 mm around the expected damage zone which is consistent with previously validated models [10,32]. One shell element through the thickness is sufficient to describe the laminate response. A prescribed displacement is imposed on one edge along the width of the OHT sample while the nodes at the opposite edge are fully constrained.

A single simulation with the described FE model in Fig. 5 takes around 2–3 min on eight CPUs. This is significantly faster than the physical test. However, considering that MCMC algorithms need a large number, often 1000s – 100,000s, of iterations (each requiring a model evaluation) to converge to the posterior density given in Eq. (1) [45], FE model evaluations $\mathcal{M}_{\text{FEA}}$ become too expensive and time-consuming for this task. More computationally-efficient simulation techniques are required to determine the probability density of FE input parameters given OHT test data. Therefore, we develop FE-informed ML surrogate models to speed up the model evaluations.

2.4. Machine learning surrogate model

The likelihood function $p(\boldsymbol{y}|\boldsymbol{\theta})$ relates the input data $\boldsymbol{\theta}$ to the OHT strength $\boldsymbol{y}$. The FEA model $\mathcal{M}_{\text{FEA}}$ described in the previous section is able to relate these features through numerical solutions of the governing partial differential equations. This ensures that the results are physically meaningful. However, the FEA approach is not fast enough to enable the large number of model evaluations or sampling required for MCMC. This motivates the use of data-driven and ML methods $\mathcal{M}_{\text{ML}}$ such as surrogate models that are constructed on the basis of physically meaningful FEA results.

To train and validate ML surrogate models for FRP composites, a large FEA dataset of around 10,000 simulation results is required based on previous investigations of combining ML and FEA for compact tension and compact compression tests [31,32]. Note that this

required dataset is still large, but is significantly less than the 100,000s of evaluations demanded by MCMC. Moreover, the training dataset can be computed in parallel.

Assuming a fixed value of Poisson's ratio $\nu = 0.32$ (c.f., [31,32]), there are three input parameter parameters: E, ε^i and G_f. These parameters $\boldsymbol{\theta} = (E, \varepsilon^i, G_f)^T$ are varied within 15,000 FE simulations to establish a relation between $\boldsymbol{\theta}$ and the simulated OHT strength $\boldsymbol{y}$ by training of neural networks. Fig. 6 shows the assumed prior probability density functions for each of these parameters. The normal distribution of the laminate elastic modulus $E \sim \mathcal{N}$ (62000, 1700) with a mean of 62,000 MPa and a standard deviation of 1700 MPa is known from statistical experiments of the CMH-17 test program [6]. The other two probability densities for ε^i and G_f are not known and therefore we assign them uniform distributions (uninformative priors) with a wide range to avoid biasing the results towards particular parameter values.

The chosen feed-forward neural network for ML depicted in Fig. 7 consists of five hidden layers and 32 nodes per layer. An ML code developed at the University of Washington, CompML (Composites Machine Learning), is utilised [46,47]. The CompML code is written in python and based on the Tensorflow and Keras libraries with several modules for data generation, training, prediction, and visualisation of data. The ML hyper-parameters for this work are listed in Table 1. The selection of the hyper-parameters as well as the neural network architecture is done via a grid search by varying all parameters such as the optimisation algorithm and the learning rate listed in Table 1.

We deploy the ML surrogate model $\mathcal{M}_{\mathrm{ML}}$ to compute 15,000 input–output pairs (linking input parameters with open-hole strength S_{OHT}), which requires about 0.6 s. With this increased efficiency, the surrogate model $\mathcal{M}_{\mathrm{ML}}(\boldsymbol{\theta})$ can be used for MCMC to estimate the posterior $p(\boldsymbol{\theta}|\boldsymbol{y})$ according to Eq. (1). Specifically, we replace the FE model $\mathcal{M}_{\mathrm{FEA}}$ in Eq. (2) with the ML surrogate model $\mathcal{M}_{\mathrm{ML}}$ to accelerate likelihood evaluations, and therefore, enable MCMC.

2.5. Markov chain Monte Carlo

Markov chain Monte Carlo algorithms are constructed to draw samples from the Bayesian posterior $p(\boldsymbol{\theta}|\boldsymbol{y})$. In particular, the MCMC algorithm aims to solve Eq. (1) by considering the priors $p(\boldsymbol{\theta})$ of the input parameters $\boldsymbol{\theta} = (E, \varepsilon^i, G_f)^T$ shown in Fig. 6 and the test data $\boldsymbol{y}$ in Fig. 3. Note that our choice of prior assumes that the three parameters are independent. MCMC algorithms evaluate a stochastic process to generate a Markov chain of samples. In the limit of infinite samples, the samples in the Markov chain are distributed according to the posterior. The chosen MCMC algorithm in this work is the EMCEE Hammer [45] implementation of the affine invariant ensemble sampler (AIES) [48]. The AIES algorithm uses an ensemble of interacting random walks to effectively sample anisotropic posteriors. This fits the setting in this work where the values of the input parameters span several orders of magnitude. The EMCEE implementation of AIES can easily handle ML surrogate models for parameter estimation. The number of interacting random walks, referred to as the number of chains, is set to 30.

MCMC algorithms iteratively draw samples from a proposed probability density (which has to be specified) that are accepted or rejected according to their posterior probability [29]. The distribution of the set of accepted samples converges to the posterior as the number of samples increases. In practice, the total number of samples to draw and those that are discarded to account for initialisation (termed *burn-in length* [29,35]) must be determined by the user. In [45,48], the integrated autocorrelation time (IACT), an approximation of how quickly samples in a Markov chain decorrelate, is introduced as a metric for MCMC convergence. In this work, the IACT is computed every 100 iterations of the AIES algorithm and the algorithm is stopped when the total number of samples is greater than 100 times the computed steady state IACT. Here, the steady state IACT is found by checking whether the computed IACT is within 1% of the previous value. In our simulation, the steady state IACT is 88, and thus, AIES is stopped after 8,800 iterations. Lastly, the burn-in length is chosen to be 200, and therefore the first 200 iterations of AIES are discarded to ensure that the remaining set of samples does not reflect algorithm initialisation. Overall, this yields 258,000 samples from the posterior, and required that many evaluations of the ML surrogate model.

3. Results

We first perform a global sensitivity analysis of the 15,000 FE results (linking input parameters with open-hole strength S_{OHT}) to quantify the identifiability of the input parameters. We follow the global sensitivity analysis proposed by Li et al. [49], which yields sensitivity indices that rank the importance of system inputs. Due to the assumption that the three input parameters are independent, we obtain a single sensitivity index for each input parameter listed in Table 2. A high sensitivity index (sensitivity indices are between 0% and 100%) means that this parameter has a strong influence on the predicted S_{OHT} and is therefore more likely to be practically identifiable from measurements of S_{OHT} [30,50]. Table 2 shows that the damage initiation strain ε^i with a sensitivity index of 93% is likely identifiable with the given FEA data while the laminate modulus E and the fracture energy G_f with sensitivity indices of 1% and 5%, respectively, are likely unidentifiable.

The results of the interacting random walks in MCMC for each input parameter $\boldsymbol{\theta} = (E, \varepsilon^i, G_f)^T$ are shown in Fig. 8. It can be seen that the MCMC algorithm draws samples across the specified range for the parameters associated with the laminate modulus E and fracture energy G_f assuming a normal and uniform prior, respectively. In contrast, the MCMC algorithm only explores a fraction of the uniform prior $\varepsilon^i \sim \mathcal{U}(0.6, 3.0)$ for the input parameter associated with the damage initiation strain ε^i. As mentioned in Section 2.5, we consider the MCMC algorithm converged when the IACT is within 1% of the previously calculated value.

Based on the 258,000 samples generated by MCMC, Fig. 9 compares the priors $p(\boldsymbol{\theta})$ and the obtained posteriors $p(\boldsymbol{\theta}|\boldsymbol{y})$ of each input parameter from evaluations of the ML surrogate model $\mathcal{M}_{\mathrm{ML}}(\boldsymbol{\theta})$ given the experimental test data $\boldsymbol{y}$ in Fig. 3. The normal prior of the laminate modulus E is based on experimental measurements [6]. Fig. 9(a) shows that this normal prior is carried through the three computational methods FEA, ML and MCMC resulting in an identical normally distributed posterior. The posterior for the damage initiation strain ε^i

in Fig. 9(b) shows a clear trend with the majority of strain values obtained from MCMC samples ranging between 0.6% and 1.2%. This is vastly different from the uniform prior $\varepsilon^i \sim \mathcal{U}(0.6, 3.0)$ and highlights the significance of this parameter for simulating the open-hole strength tests of FRP composites. The MCMC results with respect to the posterior of the laminate fracture energy G_f in Fig. 9(c) do not place high probabilities on specific values of G_f. While slightly more samples are drawn with energy values in the range 60–80 kJ/m^2, the resulting posterior resembles the uniform prior. More details about these findings and their correlation to the sensitivity indices shown in Table 2 are discussed in Section 5.

We randomly select 4000 parameter vectors $\boldsymbol{\theta}_i$ from the MCMC samples and evaluate the trained ML surrogate model $\mathcal{M}_{\mathrm{ML}}$ at each of the samples. Fig. 10 shows a comparison between the underlying experimental data $\boldsymbol{y}$ and the calculated OHT strength values given the posteriors of input parameters in Fig. 9. The good match between experiments and MCMC results indicate that the Bayesian estimation of input parameters was successful and that the resulting simulations can replicate the experimental distribution of open-hole strength data. However, it is important to validate these findings against experimental measurements in different test configurations. In Section 4 we apply the posteriors shown in Fig. 9 to FE simulations of OHT tests with different geometries compared to the one shown in Fig. 5.

Fig. 11 illustrates the correlation among the three parameters (E, ε^i and G_f) of the posterior samples. The two-dimensional histograms highlight the shape and intensity of each correlation. To further quantify these correlations, we calculate Pearson's Correlation Coefficient (PCC), a measure of correlation between two random variables X and Y, defined as

$$\rho_{X,Y} := \frac{\sigma_{XY}}{\sigma_X \sigma_Y}. \tag{3}$$

Here, the covariance between X and Y is denoted by σ_{XY} and σ_X and σ_Y denote the standard deviation of X and Y, respectively. Values of PCC that satisfy $\rho_{X,Y} \approx \pm 1$ indicate strong correlation between variables X and Y whereas $\rho_{X,Y} \approx 0$ indicates no correlation at all. By analysing Fig. 11 and the corresponding PCC values, we observe that the damage initiation strain ε^i and fracture energy G_f are correlated with a PCC value $\rho_{\varepsilon^i, G_f} = -0.69$. In contrast, modulus E and damage initiation strain ε^i are weakly correlated with a PCC value $\rho_{E,\varepsilon^i} = -0.35$ while G_f and E are not significantly correlated ($\rho_{G_f,E} = -0.05$).

4. Validation

In each of the two validation cases presented below, 4000 random MCMC samples are drawn to cover the estimated parameter vector $\boldsymbol{\theta} = (E, \varepsilon^i, G_f)^T$ for the three input parameters shown in Fig. 9. The FE model described in Section 2.3 applies these input parameters to evaluate the distribution of the resulting open-hole strength values for different specimen geometries. Recall that the FE mesh consists of 1 mm × 1 mm elements with one shell element through the thickness. Fig. 12 summarises the differences in OHT specimen

geometries of two validation cases compared to the specimen dimensions used for the Bayesian parameter estimations shown in Fig. 5.

4.1. Case I - change in geometry

The first validation example involves a slight change to the sample geometry shown in Fig. 12. While the underlying experimental data used to infer Bayesian parameter estimates was obtained from 36 mm wide OHT test samples with a 6 mm hole diameter, this case evaluates open-hole strength in 38.1 mm wide test samples with hole diameters of 6.35 mm. Note that the width-to-hole ratio remains the same.

Fig. 13 compares the two probability density functions obtained from experiments reported in [51] and 4000 FEA simulations. The experimental data is generated by 19 samples from three different manufacturing batches [51] using the same IM7/8552 CFRP laminates with areal density of 190 g/m^2 as described in Section 2. The good qualitative match between simulation and experiments shown in Fig. 13 is confirmed by comparing quantitative data to the mean and coefficient of variation of the open-hole strength values. Table 3 highlights that both quantitative measures can be accurately simulated with differences of less than 1%.

4.2. Case II - size effects

The second validation case investigates the size effects in scaled OHT tests. Green et al. [40] studied three different OHT geometries, here referred to as small, medium and large. The dimensions of each configuration are listed in Table 4 and illustrated in Fig. 12.

When comparing the simulation results to experimental findings in this section, it is important to note two differences from the previous validation case in Section 4.1 and the underlying experimental data for the Bayesian parameter estimation in Sections 2 and 3. First, the experimental data obtained from Green et al. [40] refers to quasi-isotropic IM7/8552 CFRP laminates with areal density of 134 g/m^2 instead of previously considered laminates with areal density of 190 g/m^2. Second, the width-to-hole ratio in the OHT samples shown in Table 4 and Fig. 12 is five compared to previously investigated samples with a width-to-hole ratio of six.

Fig. 14 shows the results of the open-hole strength simulations for the small, medium and large test specimens considering 4000 random MCMC samples obtained from the Bayesian estimation in Section 3. It can be seen that the simulations of the medium and large-scale test samples in Fig. 14(b) and (c) follow a normal distribution with mean open-hole strength values of 398 MPa and 347 MPa, respectively. While the simulation results of the small OHT test samples align with a Poisson-like distribution, a best-fit normal distribution with mean OHT strength of 434 MPa is considered in Fig. 14(a) to enable a direct comparison to experimentally measured data.

Table 5 compares these simulation results to experimental measurements. The mean values and coefficient of variation for the experimental data are calculated based on six tested specimens for each geometric configuration (small, medium and large) [40]. Note that the simulations are trained on a slightly different material system with higher areal density which can alter the simulation of ultimate OHT strength values. Nonetheless, the

comparison in Table 5 shows that Bayesian-based FEA simulations can estimate the mean OHT strength values and coefficients of variations with reasonable accuracy. It is interesting to observe that the simulations consistently result in strength predictions that are around 7%–9% lower than experimental values.

Based on the data-rich FEA evaluations of open-hole strength values shown in Fig. 14, it is possible to create meaningful boxplot graphs and to calculate virtual design allowables. Fig. 15 shows the corresponding results for the small, medium and large OHT test cases. The boxplots visualise the mean value in solid orange lines and the surrounding box indicates the 25th and 75th percentile of the open-hole strength data obtained from the Bayesian-based FEA simulations. Compared to the experimental data from Green et al. [40] shown in Table 5, the simulated 75th percentile of open-hole strength simulations aligns with the mean value obtained from experiments. For the design and certification of composites, design allowables play a central role. Typical measures are the A- and B-Basis allowables which means that at least 99% or 90% of the test data yield strength values equal to or higher than this tolerance with 95% confidence, respectively. Fig. 15 shows these design allowables for each OHT test case with simulated A-Basis allowables of 378 MPa, 364 MPa and 315 MPa for the small, medium and large test geometry, respectively. Similarly, the B-Basis allowables are 397 MPa, 379 MPa and 328 MPa.

5. Discussion

This paper combines science-based simulation (FEA in Section 2.3) with data-driven surrogate modelling (ML in Section 2.4) and probabilistic parameter estimation (MCMC in Section 2.5). Thereby, each computational technique uses readily available built-in tools in commercial and open-source software. The novelty of the presented work lies at the intersection of these three fields through the development of a complete workflow to incorporate uncertainty into efficient FE simulation of progressive damage in composite laminates. In the following, various aspects are discussed about benefits, limitations and resulting future research avenues.

5.1. Need for machine learning surrogate model

The laminate-based FE simulation of progressive damage in Section 2.3 enables real-time or even faster-than-real-time evaluations of physical mechanical tests. Here, one simulation of an open-hole tension test only takes 2–3 min on a conventional computer with eight CPUs.

As outlined in Section 2.5, the MCMC algorithm required the evaluation of 258,000 simulations. A direct coupling of MCMC with FEA would result in a computation time of approximately one year. The parallelisation of MCMC evaluations could speed up such direct coupling. While it is possible to paralellise the affine invariant ensemble sampler presented in Section 2.5, such parallelisations are nontrivial and would require access to high performance computing systems for FEA models. Most MCMC algorithms are generally not parallelisable as they rely on a single random walk through the parameter space. Section 5.5 discusses possible future extensions of the presented algorithms, including the potential for parallelisable MCMC.

The inefficient direct coupling of MCMC with FEA motivates the inclusion of data-driven surrogate modelling in form of ML outlined in Section 2.4. In this work, 15,000 FE simulations train and validate a feed-forward neural network consisting of five hidden layers and 32 nodes per layer. Evaluating the ML surrogate model $\mathcal{M}_{\mathrm{ML}}$ 258,000 times requires only 10 s. The MCMC algorithm including this efficient ML surrogate model completed in 1 h and 28 minutes on a conventional laptop (MacBook Pro with a 2.6 GHz Intel Core i7 processor).

5.2. Validation examples

It is challenging to find suitable experimental studies in the literature with sufficient test repetition and batch variation for the validation of the Bayesian-based simulation results. At best, studies present the mean value and standard deviation of open-hole tests with a limited number of test repetition. The Bayesian calibration here is based on 30 samples of IM7/8552 laminates made from seven batches [6] which promises a statistically meaningful representation of uncertainty and hence a valid calibration process.

Similarly, validation case I in Section 4.1 considers 19 samples from three manufacturing batches of the same material system. Despite the good match between experiments and Bayesian-based FEA simulations presented in Fig. 13 and Table 3 with differences of less than 1%, it should be noted that the OHT specimen geometries shown in Fig. 12(a) share a width-to-hole ratio of 6 and have similar hole diameters of 6 mm and 6.35 mm, respectively.

Therefore, a second validation case in Section 4.2 is investigated including three different OHT test geometries shown in Fig. 12(b). Table 5 and Fig. 15 show that the mean OHT strength between simulations and experiments differ by 7%–9%. The reason for this larger discrepancy is the slightly different material system with areal density of 134 g/m^2 compared to the laminates with areal density of 190 /m^2 used for the Bayesian-based calibration. This can be seen best when comparing the validation cases in Fig. 12 where the medium OHT geometry from case II resembles the geometries from case I with the only difference being the width-to-hole ratio of 6 and 5 for validation cases I and II, respectively. The mean open-hole strength values from experiments are 406.8 MPa (see Table 3) and 433 MPa (see Table 5) for cases I and II, respectively. This is a difference of about 6%–7%. Considering that a higher width-to-hole ratio increases the OHT strength according to theoretical estimates [52], experimental studies [53,54] and simulations [10], the measured OHT strength of 433 MPa in case II can be expected to increase at a width-to-hole ratio of six to equal the OHT geometry from validation case I. Therefore, the discrepancy between simulations and experiments of 7%–9% in validation case II stems from the differences in material response due to different areal densities. Hence, validation case II further demonstrates the accuracy of the Bayesian-based calibration results where mean OHT strength values are expected to be around 6%–10% lower than experimental data due to the difference in areal densities.

5.3. Posterior probability density function of input parameters

One of the novelties of the presented study is the generation of probability densities for input parameters instead of finding fixed deterministic values (e.g., a mean, mode, or

most probable point). The posteriors of the three input parameters for the laminate-based simulation of progressive damage in composites shown in Fig. 9 take vastly different shapes and ranges.

Experimental results suggest that the laminate modulus E follows a normal distribution, see Section 2.4 and [6]. This led us to define the prior as a normal distribution, and the resulting posterior remained normal, see Fig. 9(a). The unchanged posterior confirms the results obtained from the sensitivity analysis shown in Table 2 where we found that the laminate modulus E is likely unidentifiable with a low sensitivity index of 1%. Since the test data $\boldsymbol{y}$ shown Fig. 3 only contains open-hole strength values, it can be expected that the laminate modulus E is not influential. If statistical data of entire stress–strain curves from open-hole tests were considered, the laminate modulus E would be more influential, and therefore identifiable, as it governs the slope of the stress–strain curve.

The significant peak in the posterior for the damage initiation strain ε^i in Fig. 9(b) is expected as OHT tests are known to be strength-driven with brittle failure behaviour as indicated in the stress–strain curve shown in Fig. 2(b). This also explains the posterior of the laminate fracture energy G_f in Fig. 9(c) without any clear trend indicating that the consideration of this input parameter is less significant compared to the input for damage initiation strains ε^i. These findings again align well with the results obtained from the sensitivity analysis shown in Table 2. The significant peak in the posterior of the damage initiation strain ε^i correlates with its high sensitivity index of 93%. Similarly, the low sensitivity index of 5% for the fracture energy G_f explains its almost unchanged posterior results compared to the prior uniform pdf. An interesting future study should involve statistically meaningful mechanical tests that lead to a more progressive type of damage evolution such as compact tension tests [41] to investigate whether the posteriors of the input parameters are sensitive to the underlying mechanical tests.

5.4. Virtual design allowables

As mentioned in Section 1, design allowables play an important role during the design and certification of composites. The determination of such allowables requires large and costly test programs at the coupon level with limited use at higher levels of the building block at the sub-component or the component level [6]. The large data obtained from 4000 Bayesian-based FE simulations allows calculating meaningful virtual design allowables as seen in Fig. 15.

Moreover, these FE simulations can be used to virtually move up the building block to investigate large-scale components while accounting for inherent material uncertainties of composites. Instead of empirical estimations at the structural level, the Bayesian approach presented here promises to seemingly transition from coupon-level studies to more application-relevant test cases without neglecting the typical range mechanical properties in composites.

5.5. Increasing complexity in models and methods

As mentioned before, each computational method uses built-in tools readily available in commercial and open-source software. Future work will investigate the potential of including more sophisticated models and methods.

The presented laminate-based FEA model yields fast simulation results with a minimal number of input parameters as shown in the bi-linear stress–strain curve in Fig. 4. More sophisticated continuum damage models with multi-linear softening curves [31,32] can increase simulation accuracy, however, it also increases the number of input parameters to be calibrated [20]. One major drawback of the laminate-based FEA model is that it neglects delamination as an explicit failure mode. Here, this can be justified by fibre-dominant failure mechanisms of dispersed quasi-isotropic $[45/0/-45/90]_{2s}$ CFRP laminates subjected to in-plane loads [41]. Other loading scenarios (such as low-velocity impact [42,44]) or stacking sequences (such as blocked $[45_4/0_4/-45_4/90_4]_s$ laminates [55]) may trigger an extended amount of delamination. More sophisticated continuum-discrete FEA models can incorporate such interlaminar failure modes at the cost of increased computation time and increased number of input parameters. Since the presented combination of FEA, ML and MCMC relies on large datasets and hence efficient evaluations of models, the computational cost is an important factor. When considering more costly FEA models, the number of ML training/validation data has to be reduced.

While the ML approach identified in this study connects inputs (i.e. selected features) to a single output (OHT strength), it is possible to train such models for any desired outcome. For example, previously, for compact compression tests, the authors trained recurrent neural networks [31], capable of predicting the entire load–displacement curve with high accuracy. Building upon the results in this study, such an approach can be implemented for predicting additional parameters other than a single strength value. In addition, by implementing other ML algorithms such as Gaussian Process Regression, the number of required FE simulations for training may be significantly reduced from the 15,000 used in this study [56,57]. This can further increase the efficiency of the current approach.

One major drawback of MCMC algorithms is their high demand for likelihood evaluations to find posteriors. The direct coupling $\mathcal{M}_{\mathrm{FEA}}$ of FEA with MCMC failed due to the lack of parallelisation as discussed in Section 5.1. The EMCEE Hammer [45] implementation of the MCMC algorithm used in this work contains a modified version that allows, in theory, to parallelise the evaluation of the sampling algorithm. Furthermore, alternative methods to MCMC, such as randomise-then-optimise [58] and variational inference [59] have been used to provide approximate solutions to Eq. (1) for high-dimensional PDE models. In addition to the need for many model evaluations, correlations between model parameters can increase the number of iterations needed for convergence [29]. While the standard approach is to increase the number of MCMC iterations, which is more than feasible when using an ML surrogate $\mathcal{M}_{\mathrm{ML}}$ as in this work, other MCMC algorithms that exploit the geometry of the likelihood function, such as Hamiltonian Monte Carlo [60], can reduce the number of required iterations. Besides choosing an alternative MCMC sampler, known correlations between parameters can be accounted for by selecting a prior that assumes dependent

parameters. One example of such a prior is a multivariate Gaussian distribution where the covariance matrix can be chosen to reflect known correlation between parameters.

6. Conclusion

This paper presents a multi-disciplinary computational approach to estimate input parameters for the finite element simulation of progressive damage in composite laminates accounting for inherent uncertainties. The input parameters are modelled as random variables and Bayes' rule is applied to learn their probability densities from given statistical test data of the outputs. Finite element informed neural networks provide highly efficient surrogate models to execute Markov Chain Monte Carlo algorithms for the Bayesian estimation of model parameters. We investigate open-hole tension tests of quasi-isotropic IM7/8552 carbon fibre reinforced polymers. The numerical results show that the combination of finite element analysis, machine learning, and Markov Chain Monte Carlo can find physically meaningful probability densities for each model input parameter. The results are successfully validated against a range of experimental test data alongside the virtual calculation of design allowables. Future work should include the consideration of mechanical tests other than open-hole tensions tests, for example compact tension tests, to determine a general set of probabilistic input parameters for the finite element simulation of progressive damage in composites and the incorporation of uncertainties.

Acknowledgments

N. Linden acknowledges support from the National Institute of Biomedical Imaging and Bioengineering (NIBIB) of the United States National Institutes of Health (NIH) under award number T32EB9380 and a UCSD Sloan Scholar Fellowship from the Alfred P. Sloan Foundation. B. Kramer acknowledges support from the Korea Institute for Advancement of Technology (KIAT) through the International Cooperative R&D program (No. P0019804, Digital twin based intelligent unmanned facility inspection solutions).

Data availability

Data will be made available on request.

References

[1]. Van Bavel B, Zhao Y, Vandepitte D, Moens D, Faes MGR. Bridging the composite meso-macro gap: a numerically efficient spatial uncertainty quantification approach. In: International conference on noise and vibration engineering. KU Leuven, Belgium, 2022.

[2]. Woigk W, Hallett SR, Jones MI, Kuhtz M, Hornig A, Gude M. Experimental investigation of the effect of defects in automated fibre placement produced composite laminates. Compos Struct 2018;201:1004–17. 10.1016/j.compstruct.2018.06.078.

[3]. Sacco C, Brasington A, Saidy C, Kirkpatrick M, Halbritter J, Wehbe R, et al. On the effect of manual rework in AFP quality control for a doubly-curved part. Composites B 2021;227:109432. 10.1016/j.compositesb.2021.109432.

[4]. Cumbo R, Baroni A, Ricciardi A, Corvaglia S. Design allowables of composite laminates: A review. J Compos Mater 2022;56(23):3617–34. 10.1177/00219983221117216.

[5]. Furtado C, Pereira L, Tavares R, Salgado M, Otero F, Catalanotti G, et al. A methodology to generate design allowables of composite laminates using machine learning. Int J Solids Struct 2021;233:111095. 10.1016/j.ijsolstr.2021.111095.

[6]. Wichita State University. Composite materials handbook volume 1 – 6. SAE International; 2012.

[7]. Reiner J, Vaziri R. Structural analysis of composites with finite element codes: An overview of commonly used computational methods. In: Beaumont P, Zweben C, editors. Comprehensive composite materials II, vol. 8. Oxford: Academic Press; 2017, p. 61–84.

[8]. Forghani A, Poursartip A, Vaziri R. An orthotropic non-local approach to modeling intra-laminar damage progression in laminated composites. Int J Solids Struct 2019;180–181:160–75. 10.1016/j.ijsolstr.2019.07.015.

[9]. Reiner J, Xu X, Zobeiry N, Vaziri R, Hallett SR, Wisnom MR. Virtual characterization of nonlocal continuum damage model parameters using a high fidelity finite element model. Compos Struct 2021;256:113073. 10.1016/j.compstruct.2020.113073.

[10]. Reiner J A practical approach for the non-local simulation of progressive damage in quasi-isotropic fibre-reinforced composite laminates. Compos Struct 2021;265:113761. 10.1016/j.compstruct.2021.113761.

[11]. Camanho P, Dávila C, De Moura M. Numerical simulation of mixed-mode progressive delamination in composite materials. J Compos Mater 2003;37(16):1415–38.

[12]. Turon A, Dávila C, Camanho P, Costa J. An engineering solution for mesh size effects in the simulation of delamination using cohesive zone models. Eng Fract Mech 2007;74(10):1665–82.

[13]. Moës N, Dolbow J, Belytschko T. A finite element method for crack growth without remeshing. Internat J Numer Methods Engrg 1999;46(1):131–50. 10.1002/(SICI)1097-0207(19990910)46:1<131::AID-NME726>3.0.CO;2-J.

[14]. Ladeveze P, LeDantec E. Damage modelling of the elementary ply for laminated composites. Compos Sci Technol 1992;43(3):257–67. 10.1016/0266-3538(92)90097-M.

[15]. Matzenmiller A, Lubliner J, Taylor R. A constitutive model for anisotropic damage in fiber-composites. Mech Mater 1995;20(2):125–52. 10.1016/0167-6636(94)00053-0.

[16]. McGregor C, Zobeiry N, Vaziri R, Poursartip A, Xiao X. Calibration and validation of a continuum damage mechanics model in aid of axial crush simulation of braided composite tubes. Composites A 2017;95:208–19. 10.1016/j.compositesa.2017.01.012.

[17]. Reiner J, Feser T, Waimer M, Poursartip A, Voggenreiter H, Vaziri R. Axial crush simulation of composites using continuum damage mechanics: FE software and material model independent considerations. Composites B 2021;225:109284. 10.1016/j.compositesb.2021.109284.

[18]. Pinho S, Iannucci L, Robinson P. Physically based failure models and criteria for laminated fibre-reinforced composites with emphasis on fibre kinking. Part II: FE implementation. Composites A 2006;37(5):766–77. 10.1016/j.compositesa.2005.06.008.

[19]. Reiner J, Feser T, Schueler D, Waimer M, Vaziri R. Comparison of two progressive damage models for studying the notched behavior of composite laminates under tension. Compos Struct 2019;207:385–96. 10.1016/j.compstruct.2018.09.033.

[20]. Fu Y-F, Reiner J Deviation-based calibration for progressive damage analysis in pultruded glass fiber reinforced composites. Int J Damage Mech 2022;31(8):1115–38. 10.1177/10567895221089655.

[21]. Fu Y-F, Reiner J Objective and automated calibration of progressive damage models for finite element simulation of fiber reinforced composites. Compos Struct 2023;307:116618. 10.1016/j.compstruct.2022.116618.

[22]. Girolami M, Febrianto E, Yin G, Cirak F. The statistical finite element method (statFEM) for coherent synthesis of observation data and model predictions. Comput Methods Appl Mech Engrg 2021;375:113533. 10.1016/j.cma.2020.113533.

[23]. Van Vinckenroy G, de Wilde W. The use of Monte Carlo techniques in statistical finite element methods for the determination of the structural behaviour of composite materials structural components. Compos Struct 1995;32(1):247–53. 10.1016/0263-8223(95)00055-0.

[24]. Goda K, Phoenix S. Reliability approach to the tensile strength of unidirectional CFRP composites by Monte-Carlo simulation in a shear-lag model. Compos Sci Technol 1994;50(4):457–68. 10.1016/0266-3538(94)90054-X.

[25]. Xu X, Wisnom MR, Hallett SR. Deducing the R-curve for trans-laminar fracture from a virtual over-height compact tension (OCT) test. Composites A 2019;118:162–70. 10.1016/j.compositesa.2018.12.027.

[26]. Malgioglio F, Pimenta S, Matveeva A, Farkas L, Desmet W, Lomov SV, Swolfs Y. Microscale material variability and its effect on longitudinal tensile failure of unidirectional carbon fibre composites. Compos Struct 2021;261:113300. 10.1016/j.compstruct.2020.113300.

[27]. Nam KM, Park K-J, Shin S-J, Kim SJ, Choi IH. Estimation of composite laminate design allowables using the statistical characteristics of lamina level test data. Int J Aeronaut Space Sci 2015;16:360–9.

[28]. Gelman A, Carlin JB, Stern HS, Rubin DB. Bayesian data analysis. Chapman and Hall/CRC; 1995.

[29]. Smith RC. Uncertainty quantification: Theory, implementation, and applications, vol. 12. SIAM; 2013.

[30]. Linden NJ, Kramer B, Rangamani P. Bayesian parameter estimation for dynamical models in systems biology. In: Saucerman JJ, editor. PLOS Comput Biol 2022;18(10):e1010651. 10.1371/journal.pcbi.1010651. [PubMed: 36269772]

[31]. Reiner J, Vaziri R, Zobeiry N. Machine learning assisted characterisation and simulation of compressive damage in composite laminates. Compos Struct 2021;114290. 10.1016/j.compstruct.2021.114290.

[32]. Zobeiry N, Reiner J, Vaziri R. Theory-guided machine learning for damage characterization of composites. Compos Struct 2020;246:112407.

[33]. Reiner J Finite element analysis combined with machine learning to simulate open-hole strength and impact tests of fibre-reinforced composites. Int J Comput Methods 2241005. 10.1142/S0219876222410055.

[34]. Sivia D, Skilling J. Data analysis: A bayesian tutorial. OUP Oxford; 2006.

[35]. Owen AB. Monte Carlo theory, methods and examples. 2013, https://artowen.su.domains/mc/.

[36]. Adeli E, Rosić B, Matthies HG, Reinstädler S, Dinkler D. Bayesian parameter determination of a CT-Test described by a viscoplastic-damage model considering the model error. Metals 2020;10(9).

[37]. Joshi A, Thakolkaran P, Zheng Y, Escande M, Flaschel M, De Lorenzis L, et al. Bayesian-EUCLID: Discovering hyperelastic material laws with uncertainties. Comput Methods Appl Mech Engrg 2022;398:115225. 10.1016/j.cma.2022.115225.

[38]. Wu T, Rosic B, De Lorenzis L, Matthies H. Parameter identification for phase-field modeling of fracture: a Bayesian approach with sampling-free update. Comput Mech 2021;67:435–53. 10.1007/s00466-020-01942-x.

[39]. Green PL, Worden K. Bayesian and Markov chain Monte Carlo methods for identifying nonlinear systems in the presence of uncertainty. Phil Trans R Soc A 2015;373(2051):20140405. 10.1098/rsta.2014.0405. [PubMed: 26303916]

[40]. Green B, Wisnom M, Hallett S. An experimental investigation into the tensile strength scaling of notched composites. Composites A 2007;38(3):867–78. 10.1016/j.compositesa.2006.07.008.

[41]. Zobeiry N, Vaziri R, Poursartip A. Characterization of strain-softening behavior and failure mechanisms of composites under tension and compression. Composites A 2015;68:29–41. 10.1016/j.compositesa.2014.09.009.

[42]. Reiner J, Zobeiry N, Vaziri R. A stacked sublaminate-based damage-plasticity model for simulating progressive damage in composite laminates under impact loading. Thin-Walled Struct 2020;156:107009. 10.1016/j.tws.2020.107009.

[43]. Forghani A, Vaziri R. Computational modeling of damage development in composite laminates subjected to transverse dynamic loading. J Appl Mech 2009;76(5). 10.1115/1.3129705,051304.

[44]. Reiner J, Zobeiry N, Vaziri R. Efficient finite element simulation of compression after impact behaviour in quasi-isotropic composite laminates. Composit. Commun 2021;28:100967. 10.1016/j.coco.2021.100967.

[45]. Foreman-Mackey D, Hogg DW, Lang D, Goodman J. Emcee: The MCMC hammer. Publ Astron Soc Pac 2013;125(925):306. 10.1086/670067.

[46]. Kim M, Zobeiry N. Machine learning for reduced-order modeling of composites processing. In: SAMPE virtual conference. Long Beach, CA, 2021.

[47]. Humfeld K, Zobeiry N. Machine learning-based process simulation approach for real-time optimization and active control of composites autoclave processing. In: SAMPE virtual conference. Long Beach, CA; 2021.

[48]. Goodman J, Weare J. Ensemble samplers with affine invariance. Commun Appl Math Comput Sci 2010;5(1):65–80.

[49]. Li G, Rabitz H, Yelvington PE, Oluwole OO, Bacon F, Kolb CE, Schoendorf J. Global sensitivity analysis for systems with independent and/or correlated inputs. J Phys Chem A 2010;114(19):6022–32. 10.1021/jp9096919. [PubMed: 20420436]

[50]. Wieland F-G, Hauber AL, Rosenblatt M, Tönsing C, Timmer J. On structural and practical identifiability. Curr Opin Syst Biol 2021;25:60–9.

[51]. Hexcel Marlett K. 8552 IM7 unidirectional prepregs 190 gsm & 35% RC qualification material property data report. Report, National Institute for Aviation Research; 2011.

[52]. Kirsch G Die theorie der elastizitat und die bedurfnisse der festigkeitslehre. Zantralblatt Verlin Deutscher Ingen 1898;42:797–807.

[53]. Lee J, Soutis C. Measuring the notched compressive strength of composite laminates: Specimen size effects. Compos Sci Technol 2008;68(12):2359–66. 10.1016/j.compscitech.2007.09.003.

[54]. Reiner J, Pizarro SO, Hadi K, Narain D, Zhang P, Jennings M, et al. Damage resistance and open-hole strength of thin veneer laminates: Adopting design and testing principles from fibre-reinforced polymers. Eng Fail Anal 2023;143:106880. 10.1016/j.engfailanal.2022.106880.

[55]. Shahbazi M An efficient virtual testing framework to simulate the progression of damage in notched composite laminates [Ph.D. thesis], The University of British Columbia, Vancouver, Canada; 2017.

[56]. Freed Y, Zobeiry N, Salviato M. Development of aviation industry-oriented methodology for failure predictions of brittle bonded joints using probabilistic machine learning. Compos Struct 2022;297:115979. 10.1016/j.compstruct.2022.115979.

[57]. Freed Y, Salviato M, Zobeiry N. Implementation of a probabilistic machine learning strategy for failure predictions of adhesively bonded joints using cohesive zone modeling. Int J Adhes Adhes 2022;118:103226. 10.1016/j.ijadhadh.2022.103226.

[58]. Bardsley JM, Solonen A, Haario H, Laine M. Randomize-then-optimize: A method for sampling from posterior distributions in nonlinear inverse problems. SIAM J Sci Comput 2014;36(4):A1895–910. 10.1137/140964023.

[59]. Blei DM, Kucukelbir A, McAuliffe JD. Variational inference: A review for statisticians. J Amer Statist Assoc 2017;112(518):859–77.

[60]. Neal RM, et al. MCMC using Hamiltonian dynamics. In: Handbook of Markov Chain Monte Carlo, vol. 2, No. 11. Chapman and Hall/CRC; 2011, p. 2.

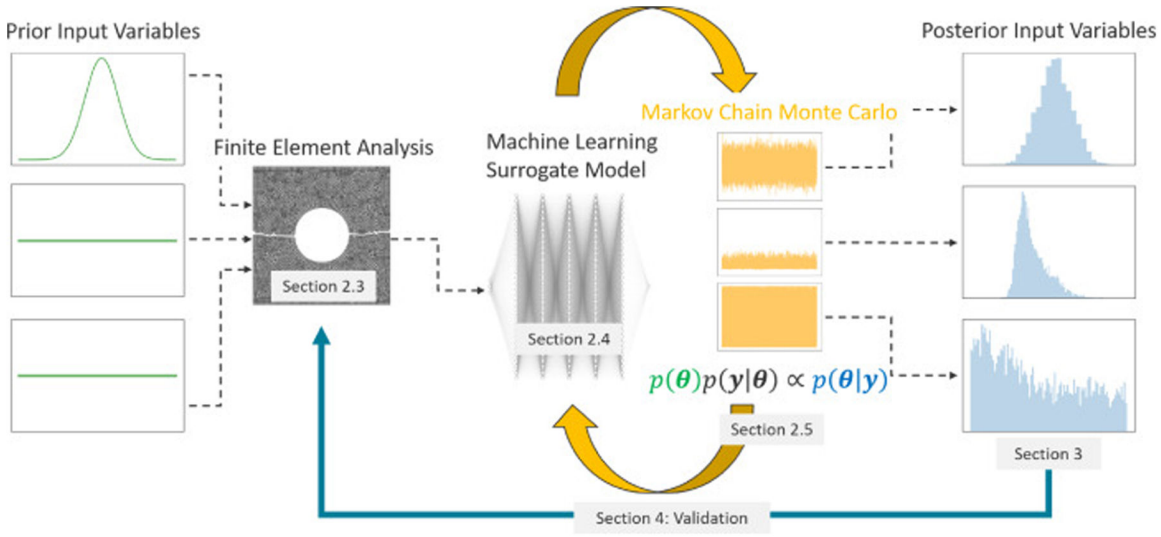

Fig. 1.

Graphical overview describing the combination of three computational methods—FEA, ML, and MCMC—to account for uncertainties in progressive damage analyses of FRP composites.

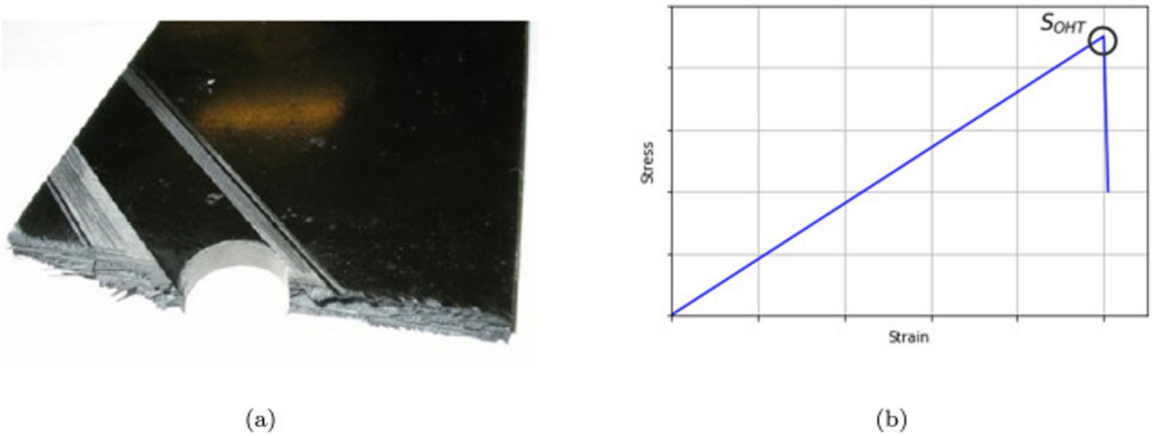

Fig. 2.
Example of (a) failed test sample [40] and (b) typical stress–strain curve obtained from open-hole tension tests of fibre reinforced laminates.

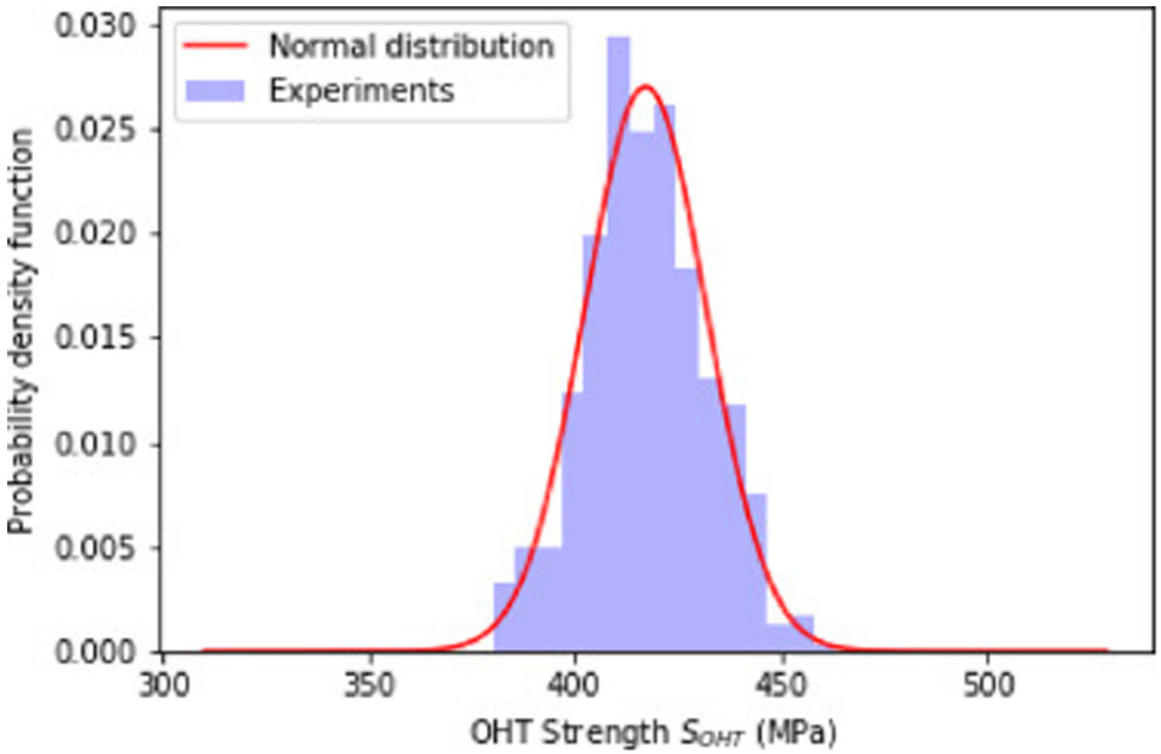

Fig. 3.

Strength evaluation of Open-Hole Tension (OHT) tests of quasi-isotropic $[45/0/-45/90]_{2s}$ IM7/8552 carbon fibre reinforced polymers [6] with 6 mm hole diameter.

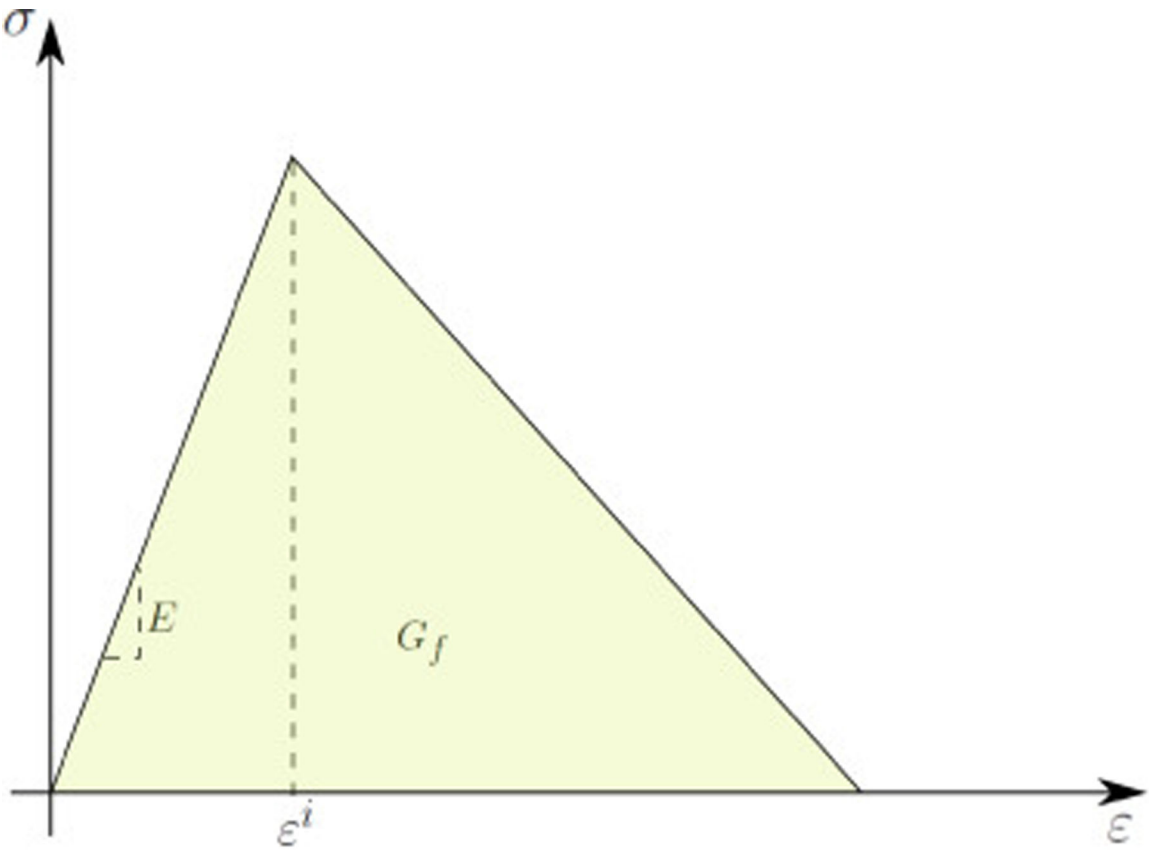

Fig. 4.

Illustration of required input parameters consisting of elastic modulus E, damage initiation strain ε^i and fracture energy G_f for the finite element simulation of progressive laminate-based damage.

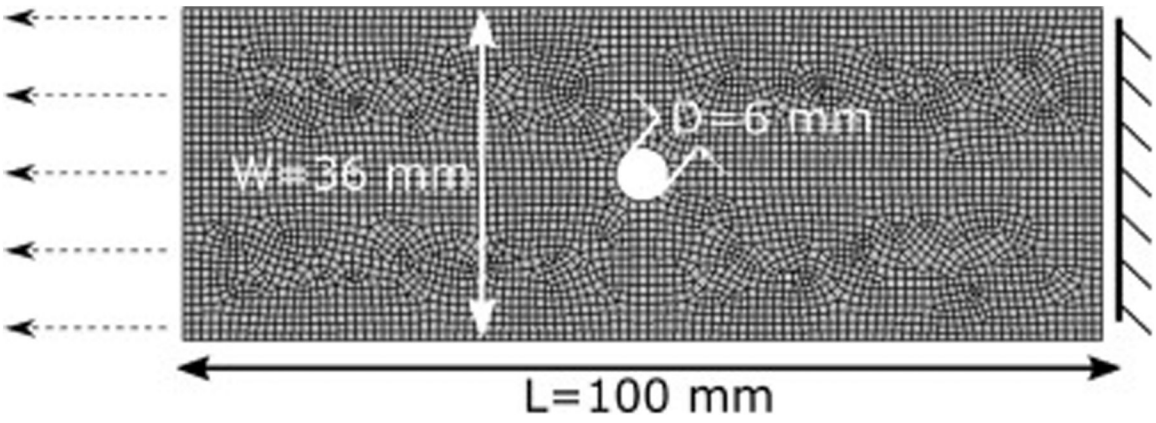

Fig. 5.

Finite element mesh, dimensions and boundary conditions used to simulate quasi-isotropic $[45/0/-45/90]_{2s}$ IM7/8552 carbon fibre reinforced polymer laminates subjected to open-hole tension tests.

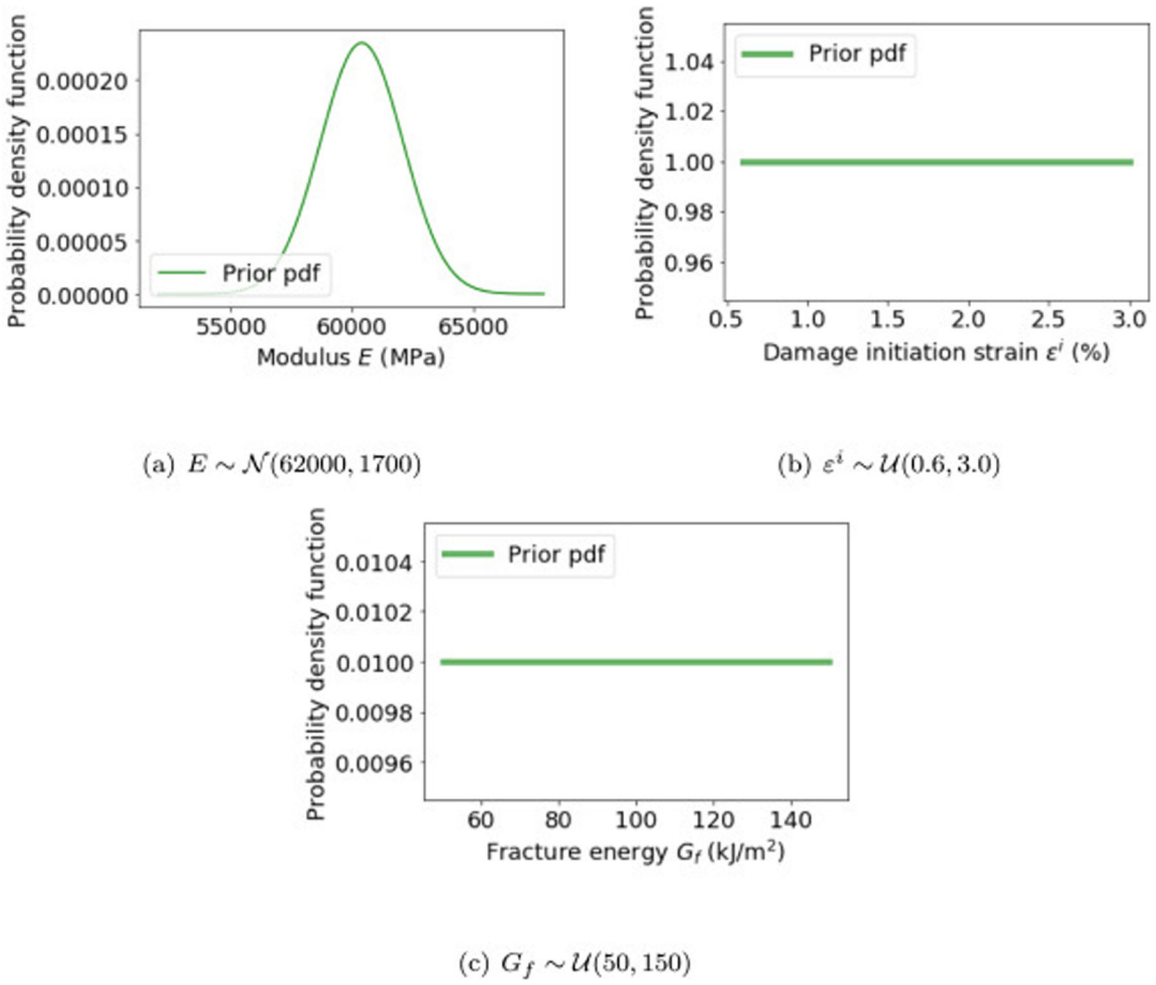

Fig. 6.

Prior probability density functions (pdf) for each input parameter to apply Bayes' rule in Eq. (1). All parameters are assumed to be independent.

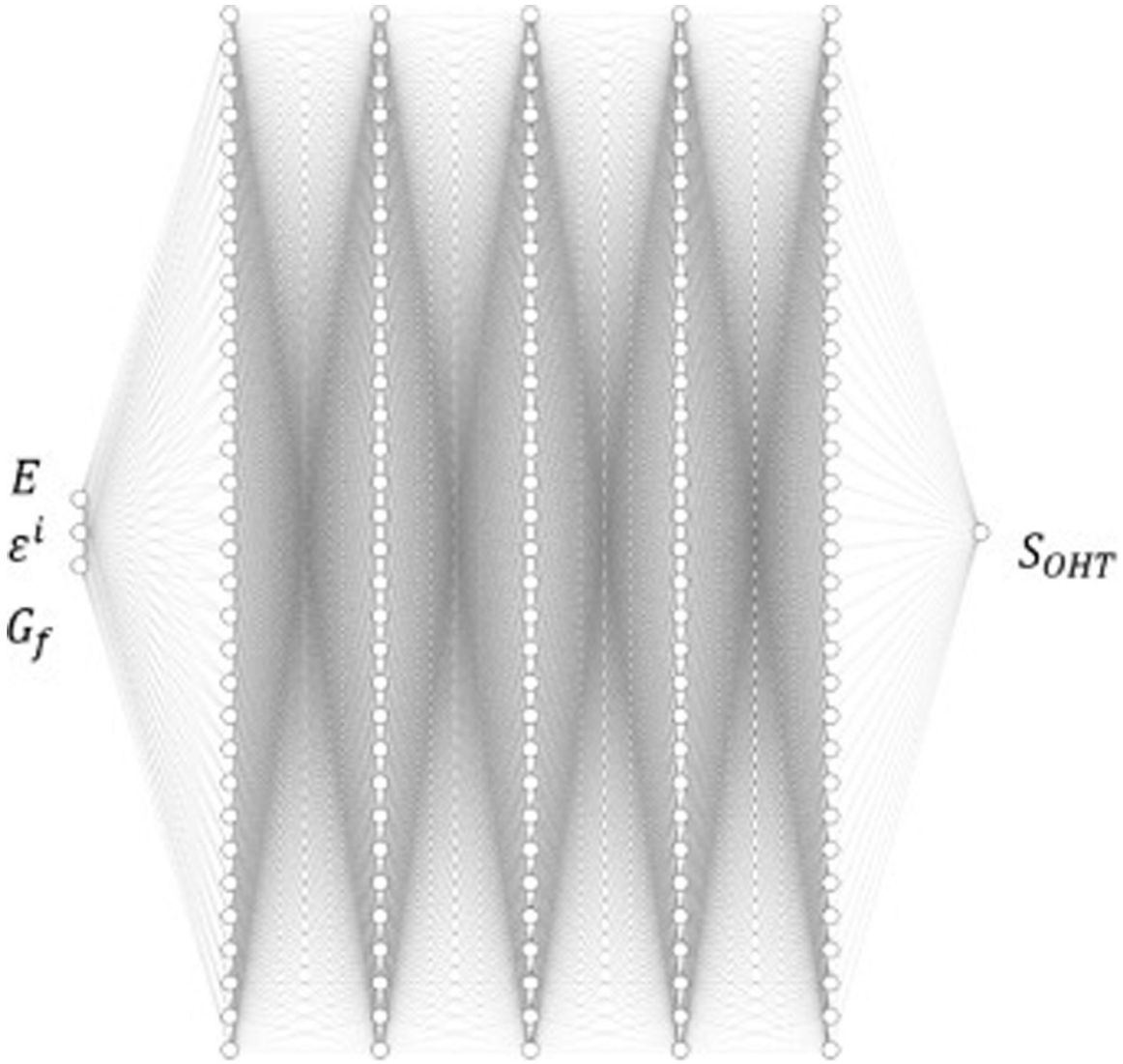

Fig. 7.

Illustration of feed-forward neural network consisting of five hidden layers and 32 nodes per layer to create efficient machine learning surrogate model linking input parameters with open-hole strength S_{OHT}.

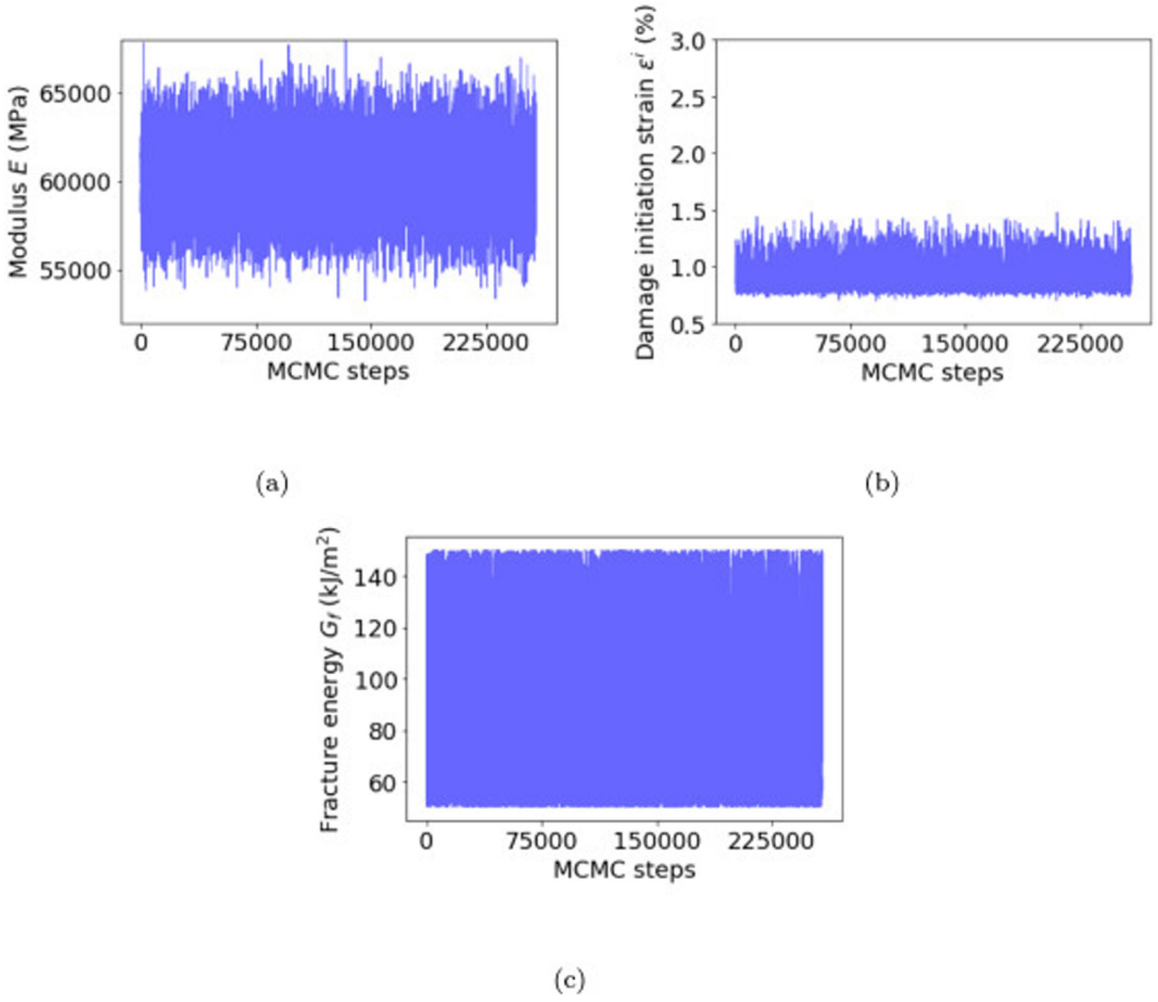

Fig. 8.

Results of interacting random walks through the parameter space $\boldsymbol{\theta} = (E, \varepsilon^i, G_f)^T$ in Markov Chain Monte Carlo (MCMC).

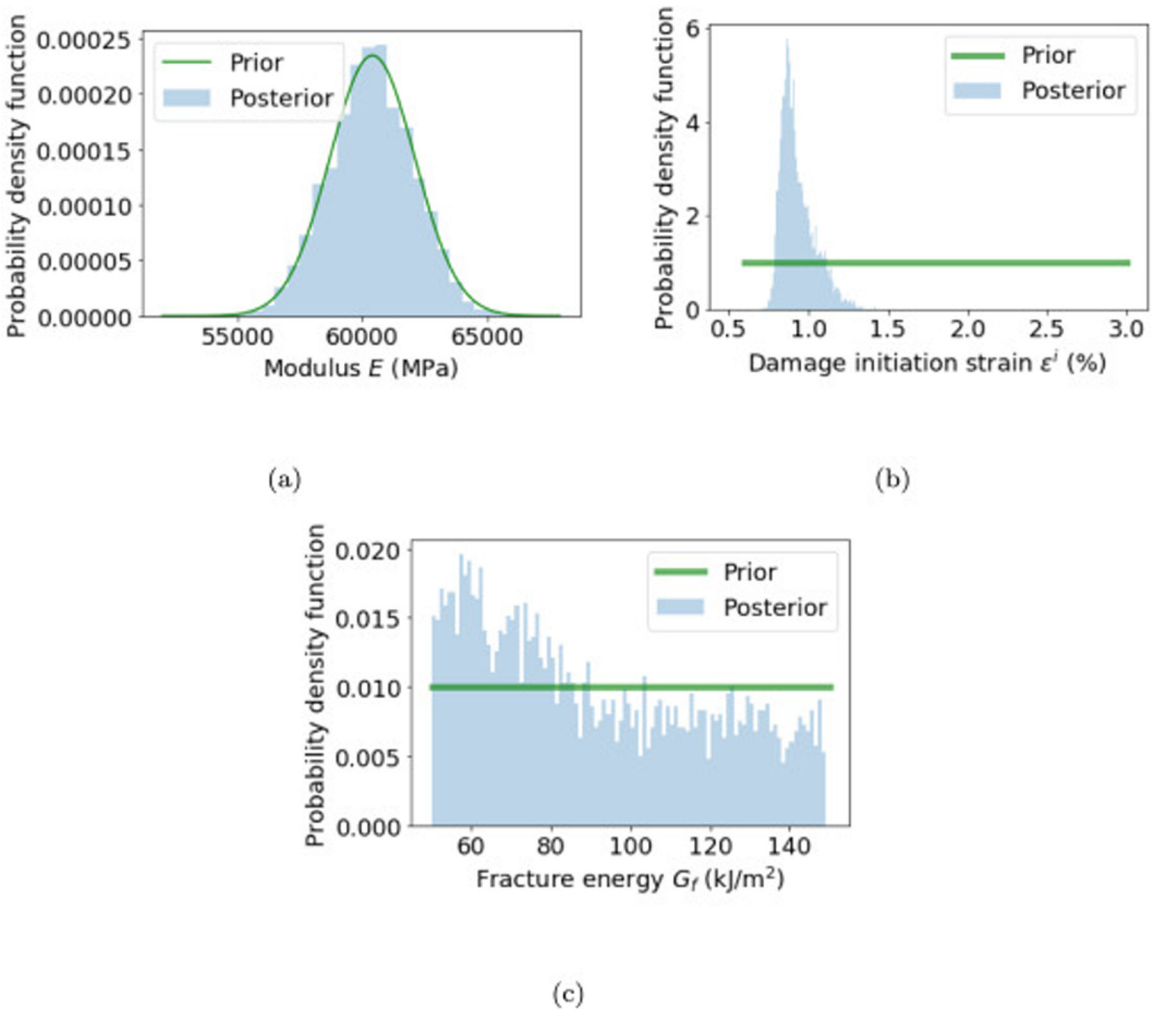

Fig. 9.

Comparison between prior and posterior for each input parameter obtained from Bayes' rule in Eq. (1).

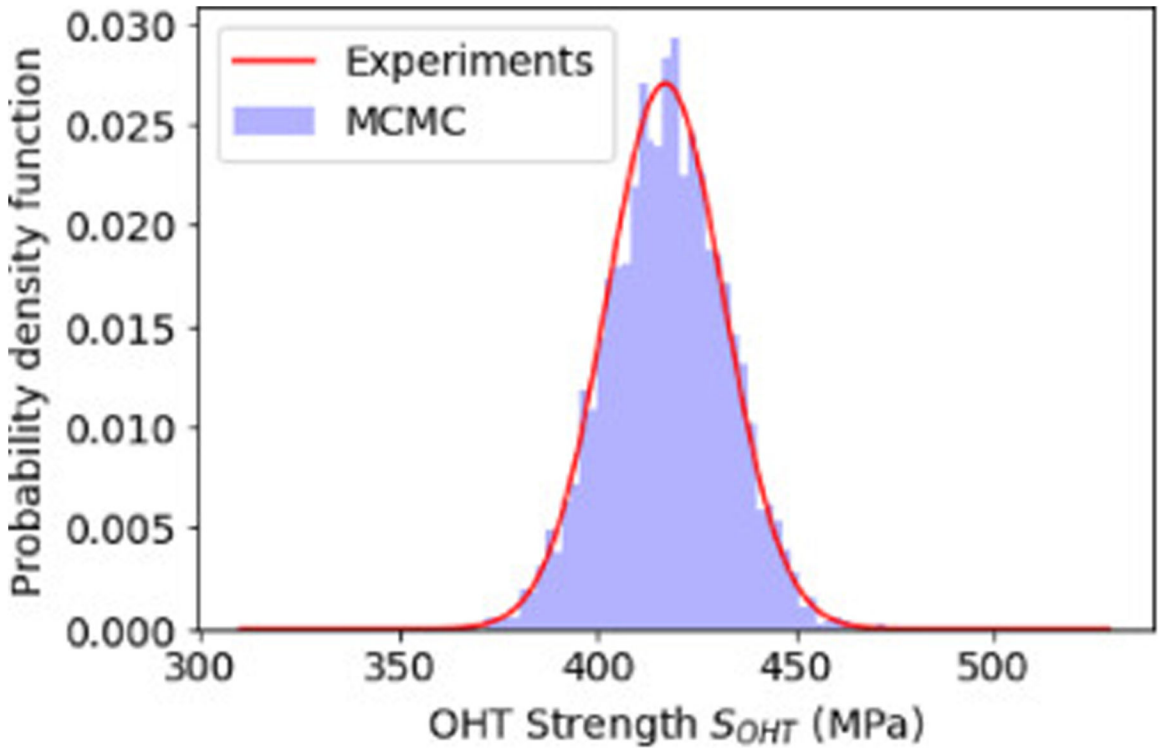

Fig. 10.
Comparison between 4000 random MCMC samples generated by the machine learning surrogate model and the underlying normally distributed experimental data used for Bayesian parameter estimation.

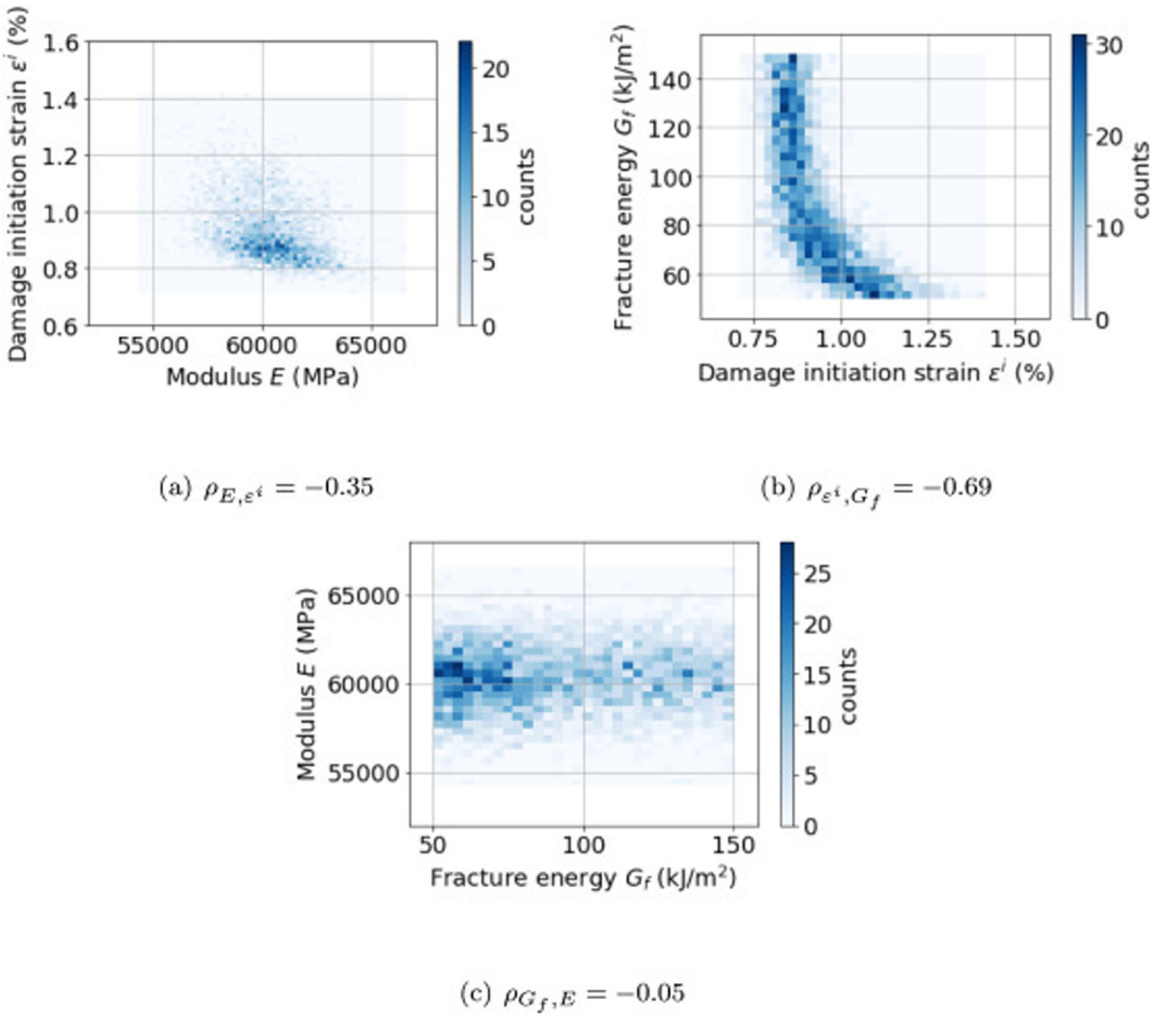

Fig. 11.

The two-dimensional histograms illustrate the shape and intensity of the correlation among input parameters of the posterior samples. We include the Pearson's Correlation Coefficient (PCC) $\rho_{X,Y}$ from Eq. (3) in the figure captions.

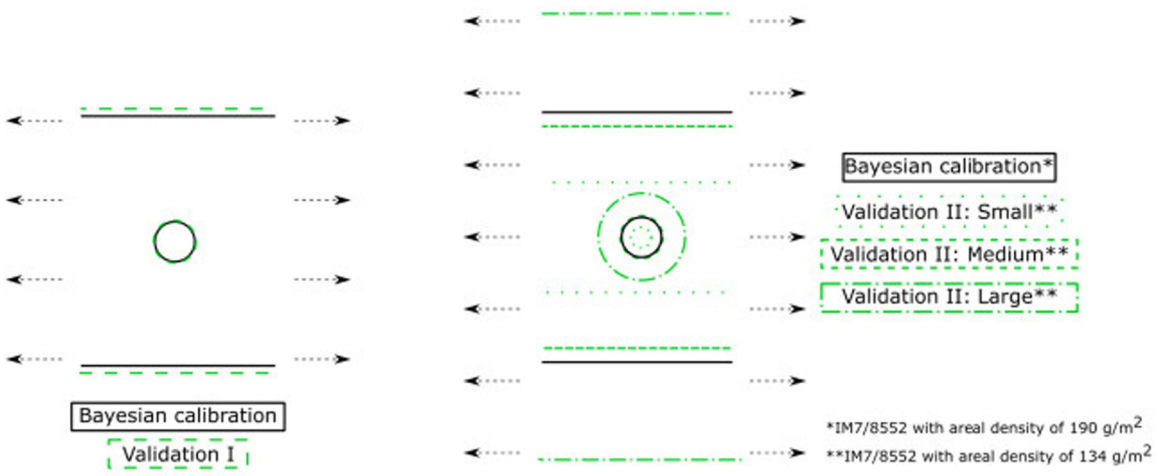

(a) Validation case I (b) Validation case II

Fig. 12.

Illustration of different open-hole tension test geometries for the validation cases of FE simulations using Bayesian-based parameters.

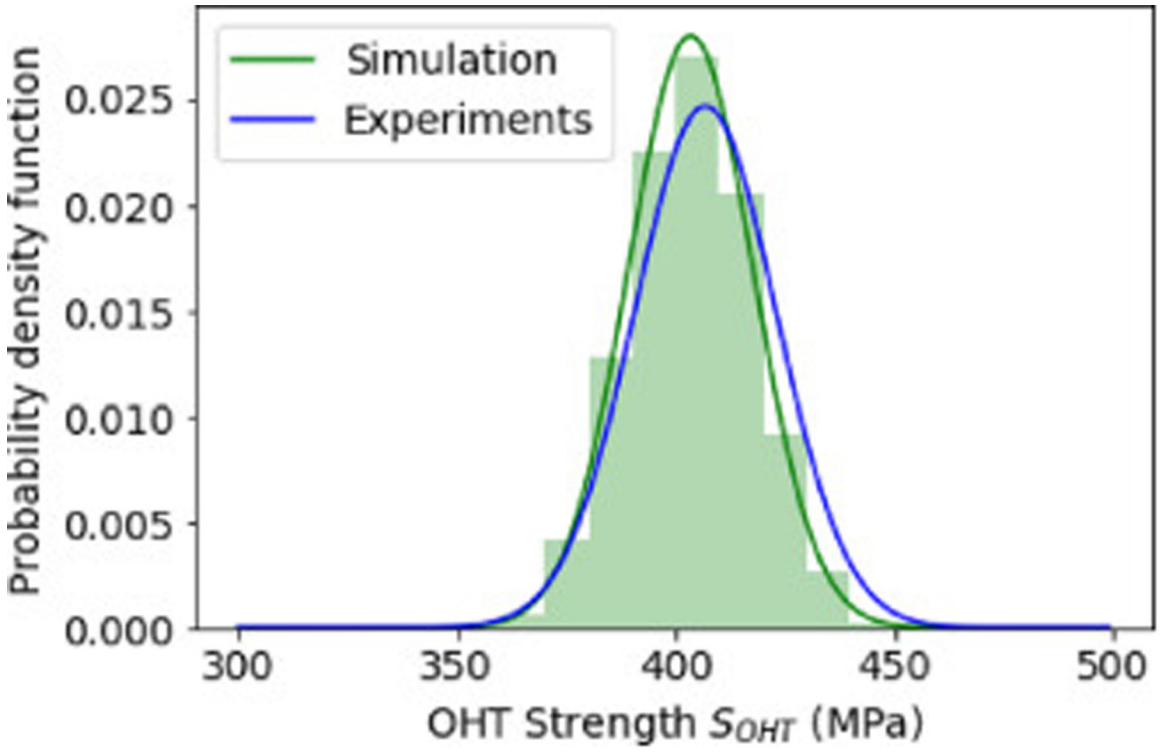

Fig. 13.

Comparison between experimental [51] and simulated open-hole strength values S_{OHT} in quasi-isotropic $[45/0/-45/90]_{2s}$ IM7/8552 carbon fibre reinforced polymers with 6.35 mm hole diameter.

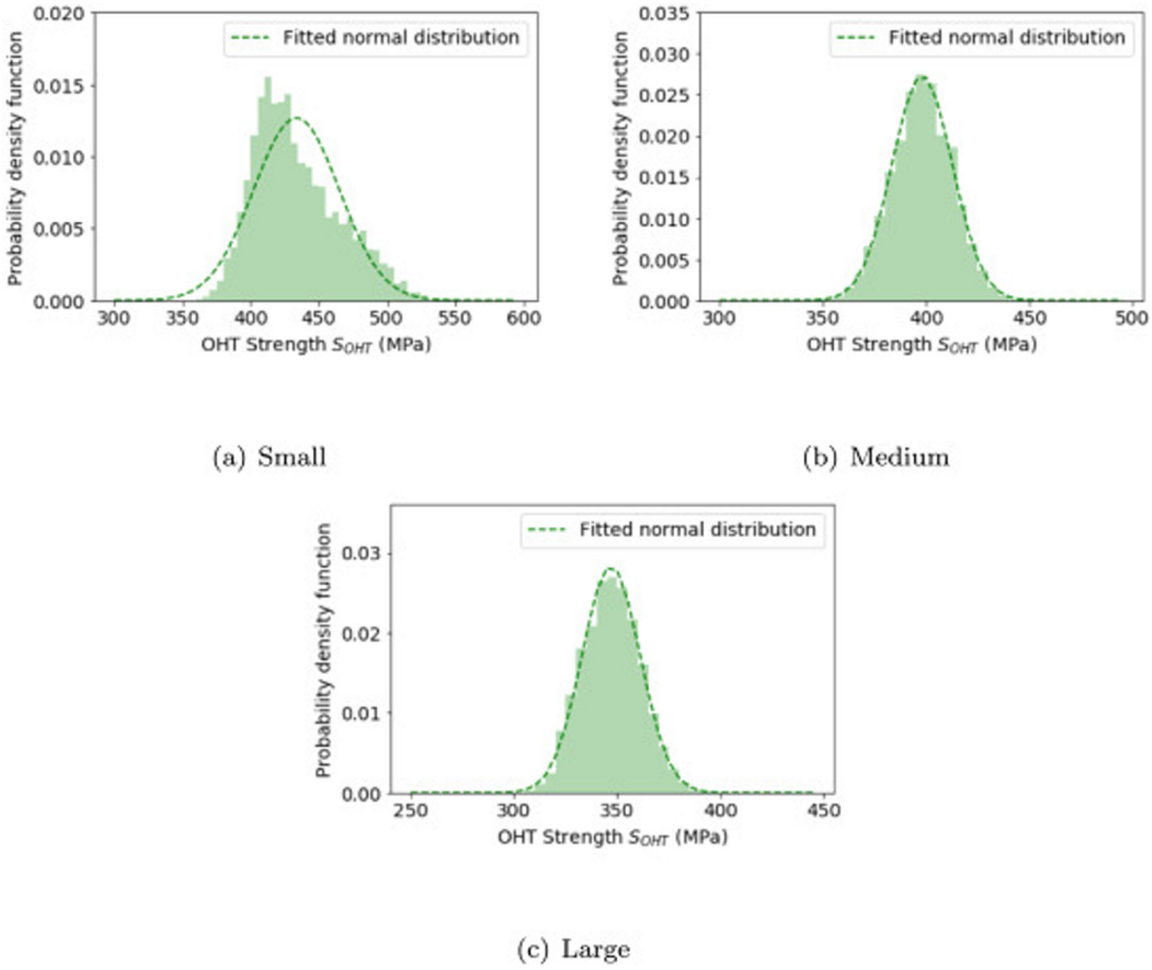

Fig. 14.

Distribution of simulated strength S_{OHT} in open-hole tension tests with small, medium and large test specimens.

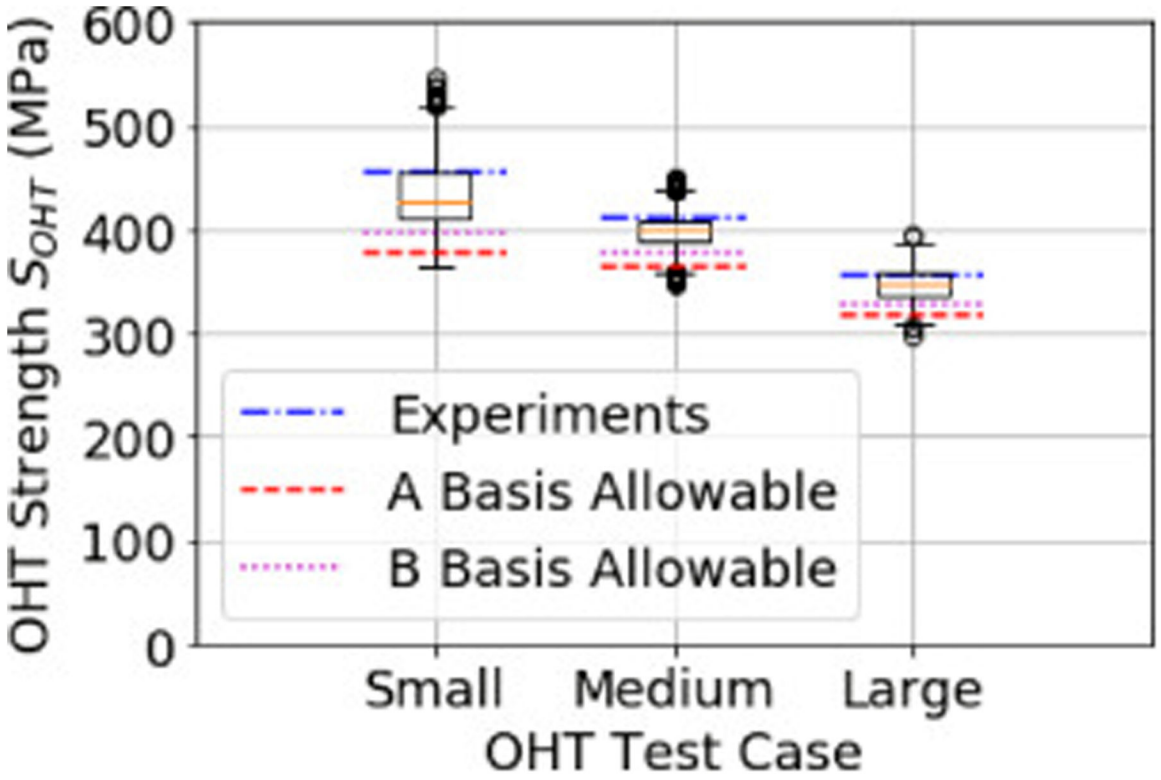

Fig. 15.

Statistical analysis and virtual design allowables from Bayesian-based finite element simulation of size effects in open-hole tension tests. Orange solid lines indicate mean values and the surrounding box indicates the 25th and 75th percentile of the open-hole strength data.

Table 1

Hyper parameters for training of feed-forward neural network depicted in Figure 7.

ML hyper parameter for training	Value
Training datapoints	10,500
Validation datapoints	4,500
Activation function	ReLU
Hidden layers	5
Nodes per layer	32
Optimiser (Adam) learning rate	0.0005
Regulariser (L2) weight	0.001
Training epochs	1,000
Batch size	200

Table 2

Results of sensitivity analysis to rank identifiability of the FE input parameters.

	E	$\boldsymbol{\epsilon^i}$	$\mathbf{G_f}$
Sensitivity Index	1%	93%	5%

Table 3

Quantitative comparison between experiments [51] and Bayesian-based finite element simulations of open-hole tension tests.

	Experiments [51]	Simulations	Difference (%)
Mean Open-hole strength (MPa)	406.8	403.4	0.8
Coefficient of variation (%)	3.98	3.53	0.4

Table 4

Dimensions of open-hole tension (OHT) specimens [40] in mm considered for validation case II.

	Hole diameter *D*	**Gauge width *W***	**Gauge length *L***
Small/Medium/Large	3.2/6.4/12.7	16/32/64	64/128/254

Table 5

Quantitative comparison between experiments [40] and Bayesian-based finite element analysis for the simulation of size effects in open-hole tension tests.

	Mean Open-hole strength (MPa)		Coefficient of variation (%)	
OHT test case	**Experiments [40]**	**Simulations**	**Experiments [40]**	**Simulations**
Small	478	434 (−9%)	3.09	7.25
Medium	433	398 (−8%)	2.03	3.66
Large	374	347 (−7%)	1.01	4.05